KeAi
CHINESE ROOTS
GLOBAL IMPACT

#### Contents lists available at ScienceDirect

# Petroleum Science

journal homepage: www.keaipublishing.com/en/journals/petroleum-science



# Original Paper

# Design of dual-functional protic porous ionic liquids for boosting selective extractive desulfurization



Jin-Rui Zhang <sup>a</sup>, Jie Yin <sup>a</sup>, Jing He <sup>a</sup>, Hong-Shun Ran <sup>a</sup>, Wei Jiang <sup>a</sup>, Hong-Ping Li <sup>a, \*</sup>, Wen-Shuai Zhu <sup>b</sup>, Hua-Ming Li <sup>a</sup>, Ming Zhang <sup>a, \*\*</sup>

- a School of the Environment and Safety Engineering & Institute for Energy Research, Jiangsu University, Zhenjiang, 212013, Jiangsu, China
- <sup>b</sup> School of Chemistry and Chemical Engineering, Jiangsu University, Zhenjiang, 212013, Jiangsu, China

# ARTICLE INFO

Article history:
Received 28 July 2023
Received in revised form
16 April 2024
Accepted 5 May 2024
Available online 15 May 2024

Edited by Jia-Jia Fei and Min Li

Keywords: Protic porous ionic liquids Extractive desulfurization Selectivity Density functional theory

#### ABSTRACT

Porous ionic liquids have demonstrated excellent performance in the field of separation, attributed to their high specific surface area and efficient mass transfer. Herein, task-specific protic porous ionic liquids (PPILs) were prepared by employing a novel one-step coupling neutralization reaction strategy for extractive desulfurization. The single-extraction efficiency of PPILs reached 75.0% for dibenzothiophene. Moreover, adding aromatic hydrocarbon interferents resulted in a slight decrease in the extraction efficiency of PPILs (from 45.2% to 37.3%, 37.9%, and 33.5%), indicating the excellent extraction selectivity of PPILs. The experimental measurements and density functional theory calculations reveal that the surface channels of porous structures can selectively capture dibenzothiophene by the stronger electrophilicity ( $E_{\rm int}$  ( $E_{\rm int}$  ( $E_{\rm int}$  surface channel/DBT) = -39.8 kcal mol $^{-1}$ ), and the multiple extraction sites of ion pairs can effectively enrich and transport dibenzothiophene from the oil phase into PPILs through  $\pi \cdots \pi$ ,  $C-H \cdots \pi$  and hydrogen bonds interactions. Furthermore, this straightforward synthetic strategy can be employed in preparing porous liquids, offering new possibilities for synthesizing PPILs with tailored functionalities. © 2024 The Authors. Publishing services by Elsevier B.V. on behalf of KeAi Communications Co. Ltd. This is an open access article under the CC BY license (http://creativecommons.org/licenses/by/4.0/).

#### 1. Introduction

Fuel has been widely used in vehicles, factories, military equipment, and other fields due to the development of the economy (Xiong et al., 2020; Zhang M. et al., 2021). However, the combustion of sulfur-containing residues present in diesel fuel can lead to the release of substantial amounts of sulfur oxides (SO<sub>X</sub>), representing a substantial threat to the overall environmental wellbeing and human habitat (Yin et al., 2023). Especially, the sulfide in the fuel can not only cause automobile exhaust catalyst poisoning but also lead to the formation of acid rain (Rajendran et al., 2020; Salah et al., 2021; Wang H. et al., 2020). Therefore, developing efficient and environmental methods to eliminate toxic sulfides is urgently needed. Hydrodesulfurization (HDS), as a well-established industrial technology, is the most traditional method for removing sulfur compounds (Salah et al., 2021). In spite of the fact that HDS is an effective means to remove sulfur compounds like sulfides, thiols

and thiophenes, it has been demonstrated that this technique is not useful for removing organosulfur compounds, including 4-Methyl dibenzothiophene (4-MDBT), and 4,6-Dimethyl dibenzothiophene(4,6-DMDBT) (Luo et al., 2021), due to the required stringent conditions (high temperature and pressure), to achieve the required desulfurization level (Zhang M. et al., 2021). Therefore, the development of non-hydrodesulfurization technology can not only effectively remove organosulfur compounds, but also improve safety and operability (Aghaei and Sobati, 2022). Extractive desulfurization (EDS) has gradually become an attractive desulfurization process based on the simplicity of operation, low energy consumption and high desulfurization efficiency (Butt et al., 2020; Salah et al., 2021).

Ionic liquids (ILs) have been deemed as a promising alternative to traditional solvents, which depends on their negligible volatility, non-flammability, thermochemical stability, high recoverability and other advantages (Smith et al., 2014). They have been widely used in various fields, such as synthesis (Zhang T. et al., 2021), organocatalytic (Jiang et al., 2020), and separation processes (Guo et al., 2017; Xu et al., 2021). Particularly, a proton can be transferred from a Brønsted acid to a Brønsted base, resulting in the formation of protic ionic liquids, which has been explored in several

<sup>\*</sup> Corresponding author.

<sup>\*\*</sup> Corresponding author. E-mail addresses: hongpingli@ujs.edu.cn (H.-P. Li), zm@ujs.edu.cn (M. Zhang).

areas such as organic synthesis, biomass conversion and separation chemistry (Jiang et al., 2021; Wang Q. et al., 2020). Moreover, protic ionic liquids exhibit distinctive biocompatibility and environmental friendliness compared with traditional ILs (Wang Q. et al., 2020). Li et al. (2012) introduced the protic ionic liquids into the EDS field. The extraction efficiency of a single extraction was more than 60% in the research. A series of amino-based protic ionic liquids has been synthesized, which showed excellent extractive ability (Li et al., 2015). Although ILs have excellent extractive performance in desulfurization, there are many obstacles to the industrial application of ILs such as their large dosage and expensive price (Abro et al., 2014).

Porous ionic liquids (PILs) is a novel kind of material that combines the high specific surface area of porous materials and the rapid mass transfer characteristics of ILs, which could effectively reduce the amount of ILs (Egleston et al., 2022; Yin et al., 2022), PILs with permanent nanopores have been considered in the separation field because of the incorporation of empty cavities into the liquid state (Li et al., 2021; Zhou et al., 2021). At present, PILs have been widely used for gas absorption based on their specific structures (Avila et al., 2021b; Greenaway et al., 2017; Zhou et al., 2021). Ma et al. (2020) reported an ionic liquid coordination cage for the capture of three gaseous chlorofluorocarbon guests. Zhou et al. (2021) obtained a PILs by combining alkyl-phosphonium halides and ZIF-8 for absorbing carbon dioxide. Very recently, the ZIF-8based PILs has been used for desulfurization, which shows fine extractive performance (Wu et al., 2021). However, the synergistic mechanism between the porous structure and ion pairs in PILs has not been mentioned. The combination of the high specific surface area of porous materials and rapid mass transfer of the ion pairs (the corona and canopy) can effectively enhance extractive capacity and reduce the number of ILs, which may become an effective means to reduce economic costs.

In this study, the clear yellow characteristic PPILs with a Brønsted acid-base pair (ion pair) were synthesized through the one-step coupling neutralization reaction (OCNR) method. Ion pairs can function as efficient capturers to enhance extraction efficiency, which could continuously transport Dibenzothiophene (DBT) to porous structures. The prepared samples exhibit highly efficient extractive capacity for DBT under mild conditions on account of the high specific surface area of porous structure and the excellent mass transfer of ion pairs. Moreover, the porous channels display excellent selectivity for DBT compared with aromatic compounds in model fuel. A synergistic extraction path with porous structure and ion pair participation was proposed based on the experimental and theoretical results.

#### 2. Experimental section

## 2.1. Chemicals

The chemical grades used to prepare model fuel are as follows: Octane (>99% GC), Dibenzothiophene (DBT, 98%), 4-Methyl dibenzothiophene (4-MDBT, 96%), 4,6-Dimethyl dibenzothiophene (4,6-DMDBT, 97%). All the above reagents were purchased from Sigma-Aldrich. The chemicals required to synthesize the extractant are as follows: Tetramethoxysilane (98%), (3-mercaptopropyl) trimethoxysilane (97%), 1,3,5-Trimethylbenzene ( $\geq$ 99.5%), Glycolic acid ethoxylate lauryl ether Mñ690 (Notes: GAELE), which were obtained from Macklin Biochemical Co. In addition, N-[2-(N-Vinylbenzylamino)ethyl]-3-aminopropyltrimethoxysilane Hydrochloride ( $\geq$ 95%, 30–40% methanol solution) (Notes: NAH) was purchased from Tokyo Chemical Industry (TCI).

#### 2.2. One-step coupling neutralization reaction (OCNR)

The PPILs were synthesized through the OCNR method of hollow silica (HS) with NAH (3-(N-Styrylmethyl-2-aminoethylamino) propyltrimethoxysilane hydrochloride) and GAELE (Poly(oxy-1,2ethanediyl)) in Scheme 1. Among them, HS is a mesoporous sphere with a cavity structure, which was synthesized using polyether F127 as a template through hydrothermal reaction (Supporting information). NAH, a silane coupling agent, is easily hydrolyzed and coupled with HS through hydroxyl groups forming the Si-O-Si bond whereas the neutralization reaction occurs between GAELE and NAH. Typically, the HS (2 wt%) was added in 10 mL of deionized water, and sonicated for 10 min. At the same time, 0.05 mol of NAH and GAELE were added to deionized water. The mixed solution reacted for 10 h at 80 °C. Finally, a pure yellow viscous liquid product was obtained in Fig. S1. In addition, the overdose NAH (0.05 mol) was weighed to couple reaction with HS (0.5 wt%). The mixture (NAH@HS) was collected by filtration and the remaining NAH was removed by washing with water and ethanol

#### 2.3. Characterization

Scanning electron microscope (SEM) and transmission electron microscope (TEM) images were obtained on JSM-6010PLUS/LA and JEOL-JEM-2100, respectively. The Micromeritics TriStar II 3020 Surface Area and Porosity Analyzer has been used to measure the N<sub>2</sub> adsorption-desorption isotherms. Fourier transform infrared (FT-IR) spectrum was measured on a Nicolet iS-50 spectrometer using Attenuated Total Reflection (ATR) method. <sup>1</sup>H nuclear magnetic resonance (<sup>1</sup>H NMR) spectrum was recorded on a Bruker DRX 400 MHz type spectrometer in deuterated chloroform. Thermogravimetric analysis and differential scanning calorimetry (TG-DSC) were tested by the NETZSCH STA 449F5.

## 2.4. Extractive desulfurization

For the preparation of model fuel, DBT, 4-MDBT and 4,6-DMDBT were dissolved in n-octane to obtain model fuel with a sulfur content of 200, 500, 800 and 1000 mg·kg<sup>-1</sup>. The desulfurization process is carried out in a two-necked flask which could maintain a constant temperature. Different ratios of PPILs and model fuel (1:1, 1:3, 1:5, 1:7) were reacted in a two-necked flask. During this process, the reaction temperature (30–50 °C) and reaction time (10–30 min) have been tested. After the reaction, precipitate the mixture for 10 min to obtain a layered solution. The model fuel on the top layer was taken out, and the residual sulfur content was detected by a gas chromatography-flame ionization detector (GC-FID).

The extraction efficiency (*EE*) was calculated based on Eq. (1) to evaluate the extractive activity of PPILs:

$$EE (\%) = \frac{C_0 - C_t}{C_0} \times 100\%$$
 (1)

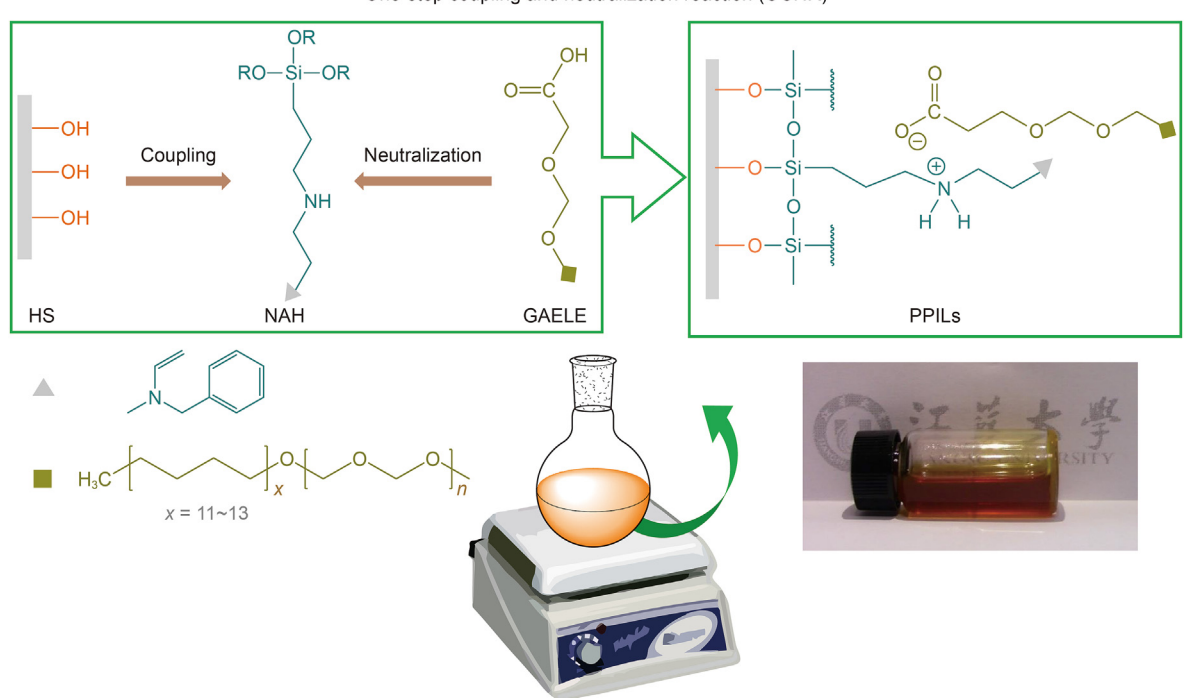
where  $C_0$  and  $C_t$  are the initial and at t time concentrations  $(\text{mg} \cdot \text{kg}^{-1})$  of the sulfur compound, respectively.

Nernst partition coefficient ( $K_N$ ) is an important parameter to evaluate the performance of extractant. Therefore, Eq. (2) has been tested to assess the capacity of PPILs:

$$K_{\rm N} = \frac{m {\rm g \cdot kg^{-1} \ sulfur \ compound_{PPILs}}}{m {\rm g \cdot kg^{-1} \ sulfur \ compound_{fuel}}} = \frac{C_0 - C_{\rm f}}{C_{\rm f}} \times \frac{m_{\rm fuel}}{m_{\rm PPILs}} \tag{2}$$

where  $C_0$ ,  $C_f$  are the initial and final concentrations (mg·kg<sup>-1</sup>) of

One-step coupling and neutralization reaction (OCNR)



Scheme 1. The synthetic procedure of the OCNR method for PPILs.

sulfur compound at any time.  $m_{\rm fuel}$  and  $m_{\rm PPILs}$  are the mass (g) of liquid fuel and PPILs, respectively (Kianpour et al., 2016; Moghadam et al., 2020).

#### 2.5. Computational details

The PPILs consist of HS and Brønsted acid-base ionic liquid. Koyama et al. (2008) reported the synthetic method of a multidimensional microporous silicate and estimated the chemical composition of the framework, which also based on the multiple tetrahedral sites. In addition, the SiO<sub>4</sub> tetrahedron was selected to construct the HS model with appropriate size in the previous work (Koyama et al., 2008; Zhang J. et al., 2020). The SiO<sub>4</sub> tetrahedron was selected to construct the HS model with appropriate size in previous studies (Yin et al., 2021; Zhang J. et al., 2020). And the SiO<sub>4</sub> tetrahedron has been used to construct an HS model with an appropriate channel structure (Zhang et al., 2023b). Based on the crystal data, a single cluster was selected as the model of HS surface channel (marked as HS-SC) in this research. As shown in Fig. S2, it is a cylindrical frame composed of multiple SiO<sub>4</sub> tetrahedrons. Besides, the simplified models of GAELE have been constructed to reduce the amount of computation, which mainly reduces the polymerization degree of ploy oxyethylene ether bond to two. The model of PPILs is shown in Fig. S3. Particularly, the models of HS-SC/ Paraxylene, HS-SC/Naphthalene and HS-SC/Phenanthrene were constructed to intuitively understand the transport mechanism of sulfur components to HS. The possible interaction sites of PPILs and DBT have been established to investigate the extraction mechanism. Related literature shows that the dispersion-corrected density functionals (e.g. B3LYP-D3) are widely used in such noncovalent systems (Gao et al., 2018; Gautam et al., 2020; Moghadam et al., 2020). Dispersion-corrected density functionals (e.g., B3LYP-D3) has been proven suitable for describing noncovalent interactions in previous work (Lv et al., 2022; Yin et al., 2023; Zhang et al., 2023b). The triple-ζ basis set with polarization functions (6-311G(d,p)) has been successfully used to describe the electronic wave function (Lv et al., 2019; Zeng et al., 2014). Therefore, computational method is high accuracy and reasonable cost to study the structures of PPILs and the extraction reactions. Hence, the computational model of B3LYP-D3 with dispersion-corrected term was employed to research the extractive desulfurization process by Gaussian 16 program (Frisch et al., 2016). Additionally, the basis set 6-311G(d,p) was used for the conformation optimization and the energy calculation.

#### 3. Results and discussion

#### 3.1. Characterization of extractant

The N<sub>2</sub> adsorption-desorption of HS and NAH has been tested to verify the coupling reaction occurring on the surface of silicon spheres without destroying the HS skeleton structure. The N<sub>2</sub> adsorption isotherms of the HS and NAH@HS show a representative type-IV(a) curve with a hysteresis loop at  $P/P^0 > 0.40$ , which is typically associated with uniform mesopores in Fig. 1(a) and Fig. S4 (Luo et al., 2019; Zhang P. et al., 2020). Besides, compared with the surface area of HS (752 cm $^2$ ·g $^{-1}$ ), the value of NAH@HS is reduced to 563  $\text{cm}^2 \cdot \text{g}^{-1}$ . It can be inferred that NAH has been attached to surface-modified HS. There are no significant changes in the shape of NAH@HS, indicating the hollow frameworks are well preserved (Yuzbashi et al., 2020; Zhang et al., 2015). The nature of PPILs and its components has determined by mass spectrometry. As shown in Fig. S8, the peaks are observed at m/z 133.01, 501.23–897.46 and 339.23 which are corresponding to the HS, GAELE and NAH. These peaks are all present in the PPILs spectrum, such as m/z 133.01, 507.35-903.59, 339.17. The result indicates that the PPILs system are consists of the HS, GAELE and NAH parts.

The <sup>1</sup>H NMR spectrum of HS to provide sufficient evidence for the coupling reactions. As shown in Fig. 1(b), the signal at 7.28 ppm belongs to the H atom of –OH in HS. The signal at 3.43 ppm

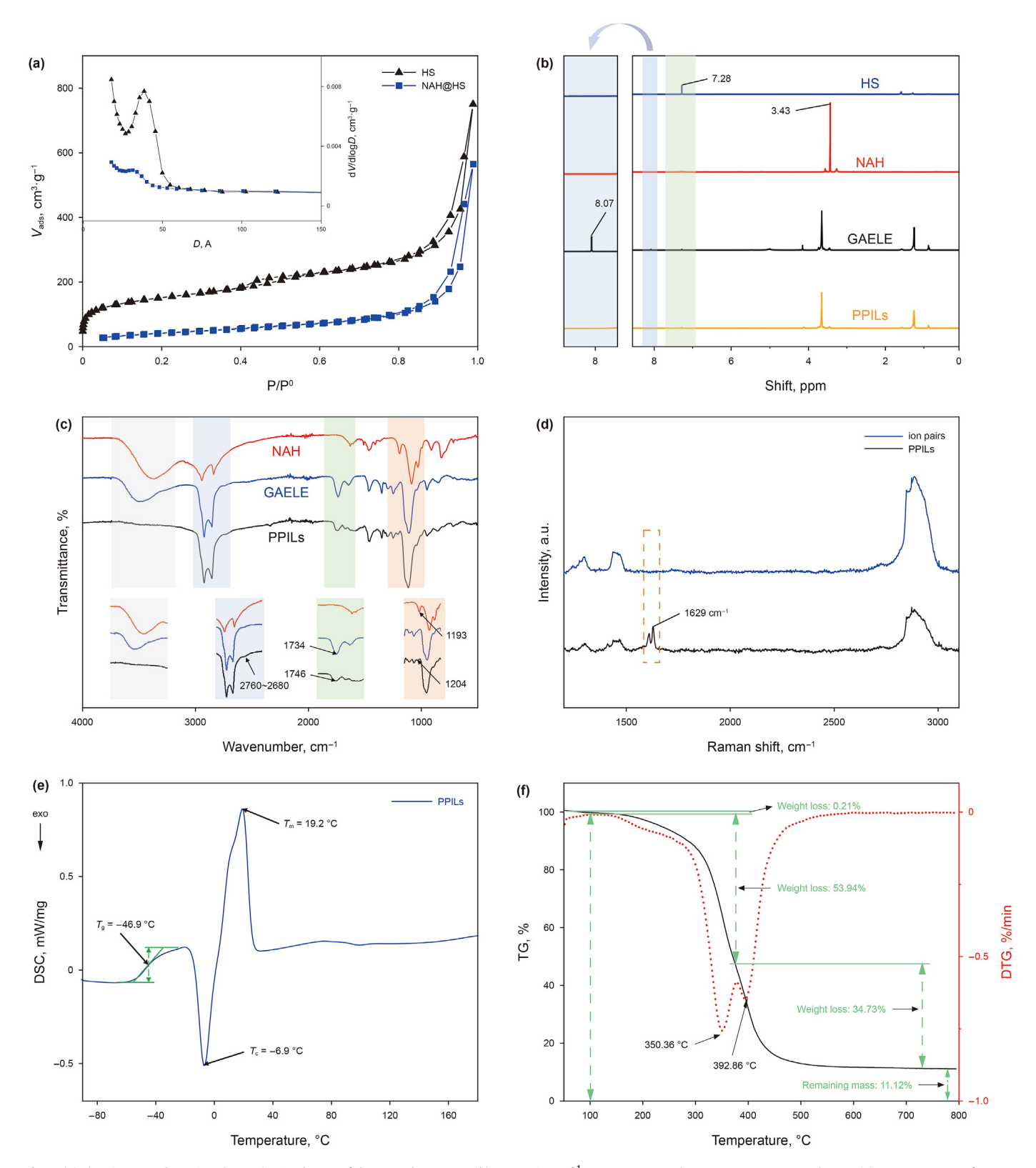


**Fig. 1.** (a) The nitrogen adsorption-desorption isotherms of the HS and NAH@HS. (b) Comparison of  $^1$ H NMR spectrum between NAH, GAELE and PPILs. (c) FT-IR spectrum of GAELE, NAH and PPILs. (d) Raman spectrum of ion pairs and PPILs. (e) The DCS curve of PPILs under  $N_2$  atmosphere at 10  $^{\circ}$ C·min $^{-1}$ . (f) TG trace and DTG curve of the PPILs under  $N_2$  atmosphere at 10  $^{\circ}$ C·min $^{-1}$ .

attributed to the H atom in methoxy group in NAH. However, all of them are disappeared after forming PPILs. The results can be inferred that the hydroxyl group in HS reacts with the methoxy group in NAH. As shown in Fig. S5, HS shows two characteristic bonds of Si–O–Si vibrational modes at 1080 and 800 cm<sup>-1</sup>, evidencing the silane precursor successfully evolved into a silica framework (El-Maghrabi et al., 2021; Luo et al., 2019; Zhang et al., 2015). Furthermore, the stretching vibration peaks of the –CH<sub>2</sub>– and –CH<sub>3</sub> backbones at 2833 and 2948 cm<sup>-1</sup> shifted to 2912 and 2981 cm<sup>-1</sup> due to the reaction of NAH and HS (Li et al., 2013; Wang et al., 2019; Zhu et al., 2016). Combining the results of <sup>1</sup>H NMR and FTIR, it can be concluded that the coupling reaction between HS and NAH has been successfully carried out.

Moreover, the signal of 8.07 ppm (GAELE) disappeared after the formation of PPILs, which belongs to the chemical shift of H atoms on the carboxyl group in GAELE. The result demonstrated that the protic transfer happens in the carboxyl group of GAELE. As shown in Fig. S6, the theoretical and experimental vibrational frequencies of the NAH were obtained, and the theoretical calculations have been corrected (scale factors = 0.964) (Zhang et al., 2022; Zhu et al., 2016). The results performance a high degree of agreement between the experimental and theoretical results. The characteristic peaks of the NAH and GAELE have been displayed in Table S1. The result shows that the peak of 1511 and 1193 cm<sup>-1</sup> in the PPILs curve belong to the deformation vibration and in-plane bending vibration of N-H, respectively. However, the vibration intensity of 1511 and 1193 cm<sup>-1</sup> have significantly weakened, with 1193 cm<sup>-1</sup> shifting to  $1204\,\mathrm{cm^{-1}}$  in Fig. 1(c). The results indicated that the NH<sup>+</sup> signals are observed in the 1511 and 1193 cm<sup>-1</sup> during the protonation of amines with acids in this work. Besides, the peak of 1734 cm<sup>-1</sup> belongs to the stretching vibration of C=O in GAELE, shifting to the 1746 cm<sup>-1</sup> due to the transfer of H protic after forming the PPILs. Therefore, it can be concluded that there is protic transfer between NAH and GAELE.

The Raman spectrum was used to further demonstrate the successful preparation of PPILs (Fig. 1(d)). To ensure the stability of the PPILs, the synthesized materials have been standing at room temperature for one week before testing. The outcomes show that the curves of ion pairs and PPILs are almost identical, except for the appearance of Raman scattering of HS caused by inelastic collisions at 1629 cm $^{-1}$  which is convincing proof of the successful synthesis of PPILs by HS and ion pairs. The DSC testing was added for PPILs to elucidate the melting or glass transition temperatures. As shown in Fig. 1(e), the glass transition temperature of PPILs is  $-46.9\,^{\circ}\mathrm{C}$  ( $T_{\mathrm{g}}$ ). The exothermic peak ( $T_{\mathrm{c}}=-6.9\,^{\circ}\mathrm{C}$ ) belongs to the crystallization peak of PPILs. And the  $T_{\mathrm{m}}$  (19.2  $^{\circ}\mathrm{C}$ ) belongs to the melting point of PPILs. The results indicate that a pure liquid material with a fixed melting point has been successfully prepared.

To probe PPILs stability and phase-transition behavior, PPILs has been characterized by DTG and thermogravimetric analysis (TG). Fig. 1(f) shows the TG analysis of the PPILs as a multi-step weight loss process. PPILs show three major stages are completely separated from one another, but the first stage is most likely caused by water that has been adsorbed in the surface water (Li et al., 2021; Ribeiro et al., 2021). The second and third steps correspond to the volatilization of the NAH and GAELE (Ramenskaya et al., 2020; Ribeiro et al., 2021). The second stage starts at 180 °C and the rate of mass loss reaches its highest at 350.36 °C, with a weight loss of 53.94% and the third step overlaps closely with the second step (starting at about 392.86 °C) with a weight loss of 34.73%. As shown in Fig. 1(f), the remaining mass of PPILs was 11.12% at the end of TG testing (800 °C). Among them, approximately 2% of the remaining mass belong to hollow silica spheres in the PPILs system. The remaining part belongs to the residue of ion pairs ([NAH][GAELE]) after the thermal degradation. This result indicated that only three

components of GAELE, NAH and HS are formed in PPILs, and no other by-products are generated. The SEM and TEM images demonstrated HS with uniform mesopore size has been dispersed in the ion pair, whose structure is well preserved in Fig. 2(a) and (b). The uniformly dispersed N, O and Si elements can be observed in the corresponding element mapping image (Fig. 2(c)). As the NAH has been grafted onto the HS, the N elements in the NAH, which are observed to be uniformly distributed, indicate that the HS is evenly dispersed in PPILs as well. In summary, PPILs have been successfully prepared through the OCNR method.

#### 3.2. Testing of extraction desulfurization conditions for PPILs

# 3.2.1. Effect of porous structure and ion pairs

Optimum extraction conditions can significantly reduce the cost of industrial applications in extraction processes (Aghaei and Sobati, 2022; Li et al., 2013). A series of factors have been investigated in detail, including the effect of extraction time and temperature, phase ratio of PPILs to model fuel, and initial sulfur concentration. For clarification of the role of HS in extractive desulfurization, PPILs (NCSS) has been synthesized by non-calcined solid silica (NCSS) while PPILs (HS) has been fabricated by hollow silica. As shown in Fig. 3(a), PPILs (HS) exhibits a higher extraction efficiency, compared to PPILs (NCSS). The extraction equilibrium can be reached after PPILs (HS) extraction for 10 min, which is much faster than PPILs (NCSS). As expected, the porous structure plays a vital role in the EDS process, which may be due to the porous framework providing a high specific surface area for PPILs. In addition, the extraction performance of HS, NAH and GAELE has been separately tested to gain more insight into the extraction ability of PPILs. As shown in Fig. 3(b), the extraction efficiency of PPILs is much higher than that of a single component (HS, NAH, GAELE). The result demonstrates the extraction ability of PPILs has significantly improved compared with the sum of all its components, indicating a synergistic effect does exist between the porous structure of HS and the Brønsted acid-base sites of ion pairs.

### 3.2.2. Extraction time and temperature

Extraction time and extraction temperature are essential parameters for measuring the performance of extractants (Li et al., 2013; Wu et al., 2021). The effect of extraction time and temperature have been investigated at a mass ratio of PPILs to model fuel of 1:5 to promote a high extractive efficiency. As shown in Fig. 4(a), the extractant PPILs achieve extraction equilibrium in 10 min with a single extraction efficiency of 42.8%. Moreover, the effect of temperature has been investigated at different temperatures (30, 40, 50 °C). The result demonstrated that the extraction capacity of DBT is not affected by the temperature changes (42.0%-44.0%). This finding indicates that the exceptional extraction efficiency was reached at 30 °C, which represents the optimum temperature. In general, PPILs reached extraction equilibrium at 10 min and 30 °C, combining the advantages of low temperature and efficient extraction for desulfurization. The most possible reason is the high specific surface area of porous structure and the rapid mass transfer of ion pairs. As shown in Table 1, the recently published literature about the EDS of ILs have been carefully compared to clarify the desulfurization capacity of PPILs. These ILs perform high EDS capacity, which has a similar structure to the ion pairs in this work, such as amino ILs, polyether group ILs, etc. The result indicates that the combination of porous materials and ion pairs not only increases the extraction rate but also maintains their extraction efficiency.

#### 3.2.3. The mass ratio of PPILs to model fuel

Higher extractive desulfurization efficiency is an important

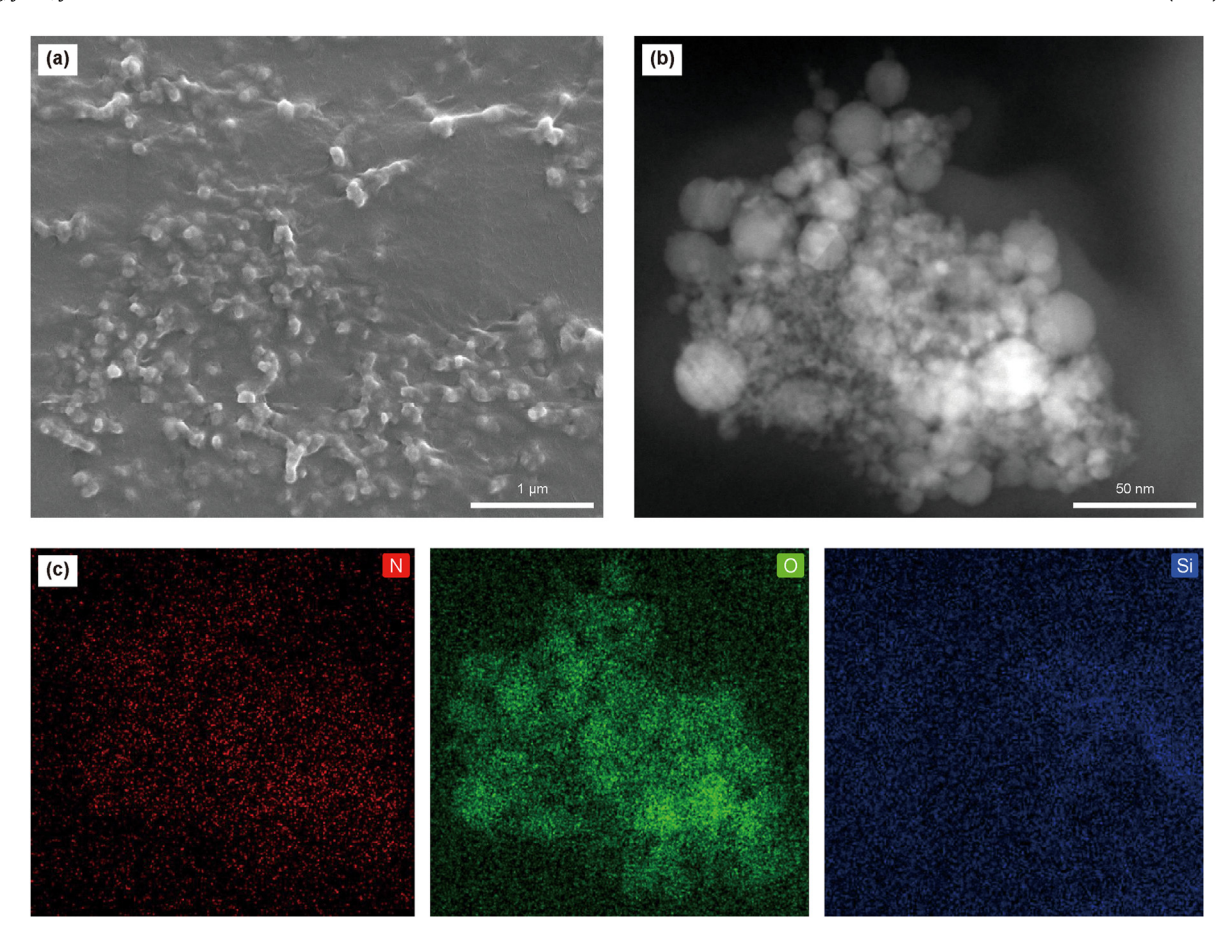
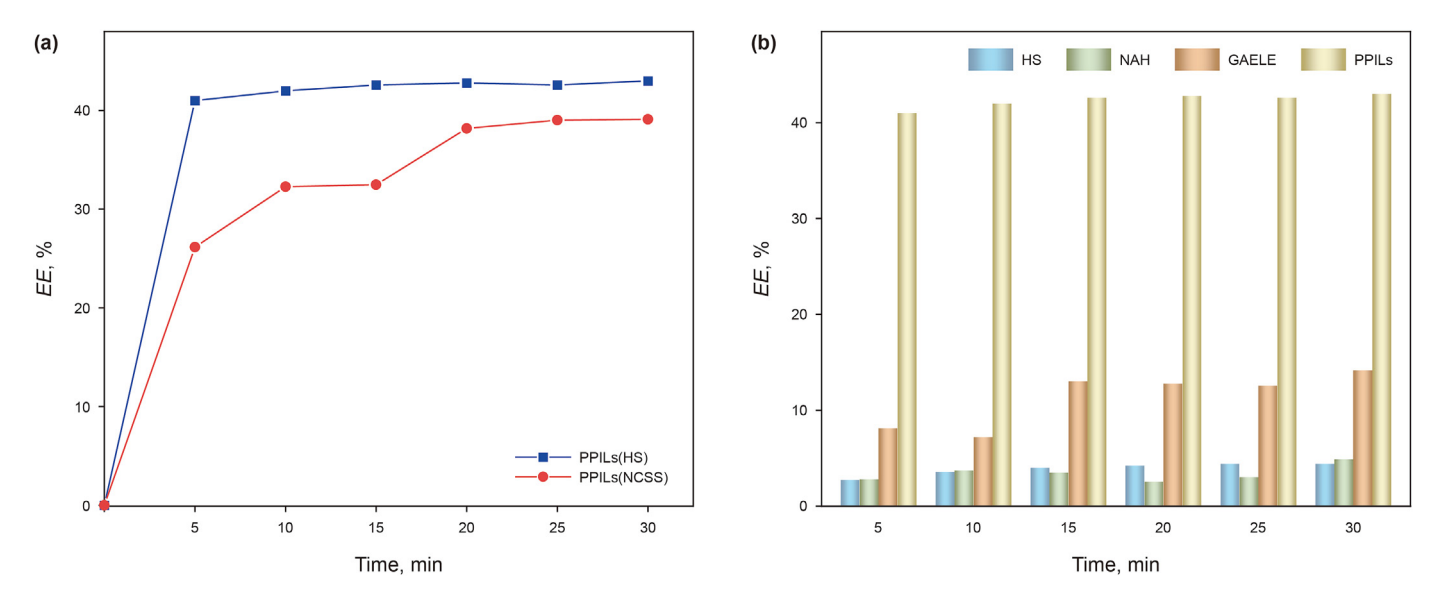


Fig. 2. (a) The SEM images of PPILs. (b) The TEM images of PPILs. (c) The elemental (N, O, Si) mapping images.



**Fig. 3.** (a) Extraction efficiency of PPILs (HS) and PPILs (NCSS). PPILs (HS) and PPILs (NCSS) respectively mean that there are synthesized by hollow silica (HS) and non-calcined solid silica (NCSS). Experimental conditions: model fuel = 0.5 g, T = 30 °C, m (PPILs (HS)): m (model fuel) = 1:5, m (PPILs (NCSS)): m (model fuel) = 1:5. (b) Extraction efficiency of PPILs and each component (HS, NAH, GAELE).

parameter for the performance of extractants, and increasing the amount of extractant is an effective means to obtain excellent efficiency (Kianpour and Azizian, 2014; Wang Q. et al., 2020). However, improving the extraction efficiency under the condition of

low-dosage PPILs is an effective way to reduce the economic cost (Aghaei and Sobati, 2022; Salah et al., 2021). Thus, the mass ratio has been tested, shown in Fig. 4(b). The results show that a larger mass ratio would benefit the desulfurization process. The single

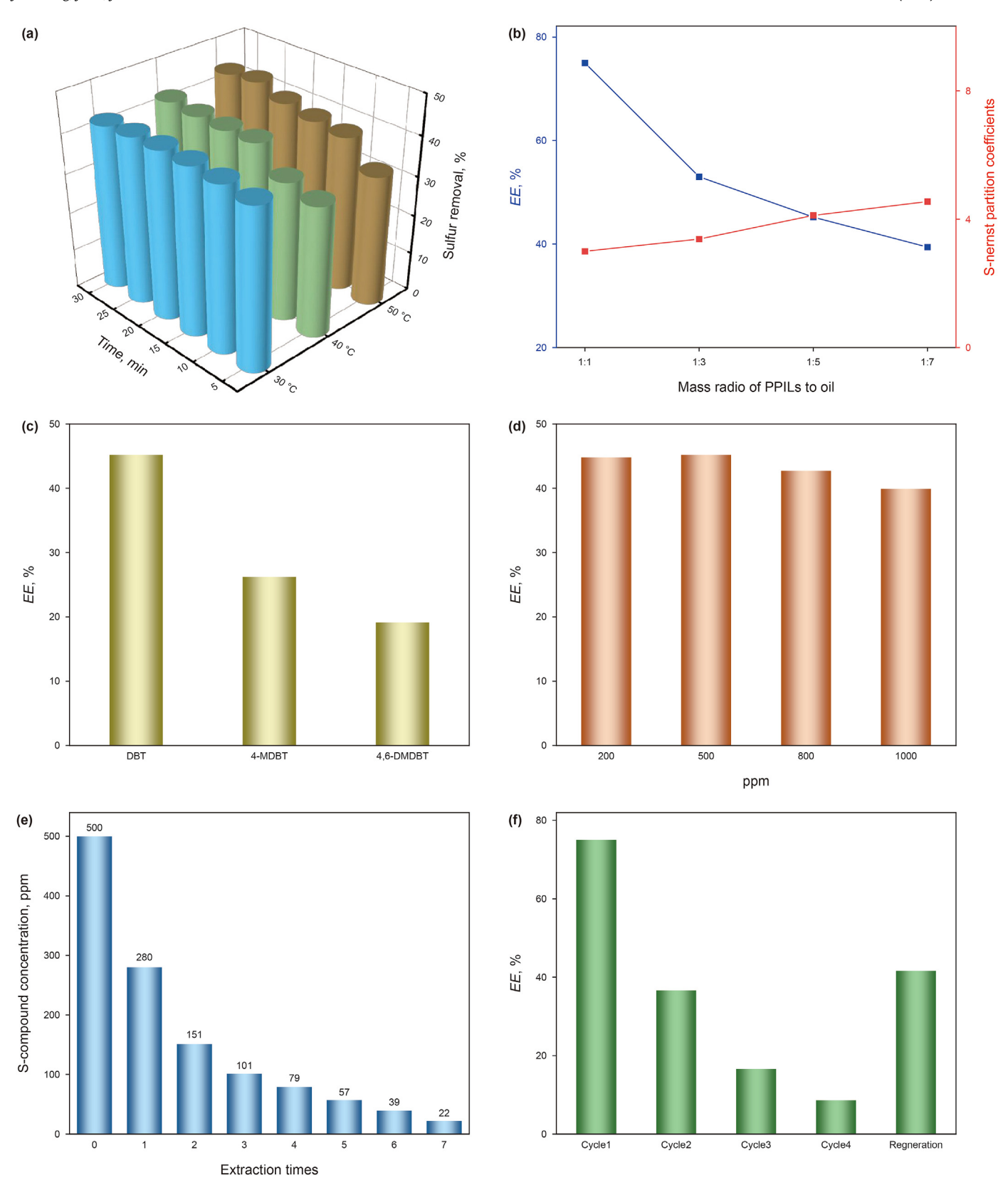


**Fig. 4.** (a) Extraction time and temperature testing of PPILs (m (PPILs): m (model fuel) = 1:5). (b) Effect of the mass ratio of PPILs to fuel on the extraction of DBT. Experimental conditions: t = 10 min,  $T = 30 ^{\circ}\text{C}$ . (c) Extraction efficiency of PPILs for DBT, 4-MDBT, 4,6-DMDBT. Experimental conditions: PPILs (m(PPILs): m (model fuel) = 1:5), t = 10 min,  $t = 30 ^{\circ}\text{C}$ . (d) The effect of initial sulfur concentration on the EDS performance of PPILs. Experimental conditions: PPILs (m(PPILs): m (model fuel) = 1:5), t = 10 min,  $t = 30 ^{\circ}\text{C}$ . (e) Concentration of DBT after multistep extraction. Experimental conditions: PPILs (m (PPILs): m (model fuel) = 1:5), t = 10 min,  $t = 30 ^{\circ}\text{C}$ . (f) The extraction efficiency of DBT during several times reuse (cycles 1–4) and after regeneration of PPILs. Experimental conditions: PPILs (m (PPILs): m (model fuel) = 1:1), t = 10 min,  $t = 30 ^{\circ}\text{C}$ .

**Table 1**Comparison of the extraction capability between PPILs and ILs materials with similar structure.

Entry	Extracting agent	Extractant conditions	$K_{\rm N}$	Ref.
1	PPILs	$T = 30  ^{\circ}\text{C}, t = 10  \text{min},  \text{E/F} = 1.5$	4.12	This work
2	PEA/FA complex	$T = 30  ^{\circ}\text{C}, t = 5  \text{min, E/F} = 1:1$	2.38	Zhu et al. (2020)
3	Polyether-based IL	$T = 30  ^{\circ}\text{C}, t = 5  \text{min, E/F} = 3.5:1$	3.24	Yu et al. (2016)
4	Polyethylene glycol	$T = 25  ^{\circ}\text{C}, t = 60  \text{min},  \text{E/F} = 1:1$	1.40	Meng et al. (2020)
5	[DBU][Im]	$T = 25  ^{\circ}\text{C}, t = 10  \text{min},  \text{E/F} = 1:2$	3.81	Ren et al. (2018)
6	[TMG][Im]	$T = 25  ^{\circ}\text{C}, t = 10  \text{min},  \text{E/F} = 1:1$	2.04	Ren et al. (2018)
7	[MTPPBr][TetEG]	$T = 20  ^{\circ}\text{C}, t = 30  \text{min},  \text{E/F} = 1:1$	0.82	Sudhir et al. (2019)
8	[TEtA][Fo]	$T = 30  ^{\circ}\text{C}, t = 10  \text{min},  \text{E/F} = 1:1$	1.08	Wang et al. (2016)
9	[TEtA][Ac]	$T = 30  ^{\circ}\text{C}, t = 10  \text{min},  \text{E/F} = 1:1$	1.72	Wang et al. (2016)
10	[TEtA][Pr]	$T = 30  ^{\circ}\text{C}, t = 10  \text{min},  \text{E/F} = 1:1$	2.14	Wang et al. (2016)
11	PPIL-AM	$T = 30  ^{\circ}\text{C}, t = 30  \text{min},  \text{E/F} = 1:2$	0.27	Zhang et al. (2023b)
12	PPIL-2AM	$T = 30  ^{\circ}\text{C}, t = 30  \text{min},  \text{E/F} = 1:2$	0.17	Zhang et al. (2023b)
13	PPIL-Ph	$T = 30  ^{\circ}\text{C}, t = 30  \text{min},  \text{E/F} = 1:2$	2.21	Zhang et al. (2023b)
14	OS-PIL	$T = 50  ^{\circ}\text{C}, t = 30  \text{min},  \text{E/F} = 1.5$	4.22	Zhang et al. (2023a)

Note: m(Extractant)/m(Fuel) is denoted as E/F.

extraction efficiency of PPILs reaches 75.0% when the ratio of extractant to model fuel is 1:1. However, the  $K_{\rm N}$  only increased from 3.00 to 4.25, indicating the mass ratio of extractant to fuel has lightly influenced the extraction performance. The proper proportion of extractants and fuel plays a crucial part in enhancing the efficiency of industrial applications. Therefore, the mass ratio of extractant to model fuel is set as 1:5 in the following experiment to balance the extraction efficiencies and consumption.

#### 3.2.4. Extraction of different sulfur compounds

Although PPILs perform excellently in the extractive of DBT. There is a wide range of sulfur compounds in real fuels. Investigating the selectivity of extractants for sulfur compounds has significant value for the research (Wang Q, et al., 2020; Xu et al., 2021). As shown in Fig. 4(c), three kinds of sulfur compounds (DBT, 4-MDBT, 4,6-DMDBT) have been tested. The extraction capacity of PPILs follows the order DBT > 4-MDBT >4,6-DMDBT, which is consistent with their electron affinity and electrophilicity (Li et al., 2019). Compared with that of 4-MDBT and 4,6-DMDBT, DBT possesses a higher electron affinity and electrophilicity resulting in the efficient interaction (Li et al., 2016; Xu et al., 2021).

#### 3.2.5. Effect of DBT initial concentration

The extraction efficiency of PPILs for multiple initial concentrations of sulfur is an important parameter to evaluate the industrial application prospects (Butt et al., 2020). The effect of initial sulfur concentration (200, 500, 800 and 1000 mg·kg<sup>-1</sup>) has been investigated on the removal efficiencies of DBT with PPILs. The extraction efficiencies of DBT decrease slightly with the increase of sulfur concentration in Fig. 4(d), which may be caused by the saturated extraction of PPILs (Wu et al., 2021). The result means that PPILs can be used to extract fuel with various sulfur concentrations, making it attractive in the industrial extraction field (Wang Q. et al., 2020; Zhao et al., 2016).

## 3.2.6. Multistage extraction

Multistage extractive strategy is an effective approach to reach deep desulfurization (Jiang et al., 2015; Kianpour and Azizian, 2014). Specifically, after the single extractive of DBT, the extractant was separated and fresh PPILs was added. The result is shown in Fig. 4(e), the sulfur content could be reduced from 500 to  $22~{\rm mg\cdot kg^{-1}}$  (EE=95.6%) after seven extractions, indicating the prepared PPILs show excellent extraction abilities for DBT.

## 3.2.7. Recycling and regeneration

The reuse and regeneration of extractants are extremely important for their industrial application. The extraction capacity of

PPILs is determined during the recycling process in several runs. As shown in Fig. 4(f), the EE of PPILs gradually decreases with the increase in cycle times. After being reused in the extraction process for four steps, the PPILs approach saturation and require recovery. Petroleum ether is used for regeneration extractants. Add the used PPILs to petroleum ether, stir vigorously at room temperature at 30 °C and centrifuge for 5 min. Then petroleum ether has been removed by rotary evaporator. This process has been repeated several times. The results showed that the extraction performance of the regenerated extractant has significantly improved, although it's still lower than that of the fresh PPILs, which may be attributed to the special structure of PPILs. The regeneration and cyclic stability of PILs have few been reported so far due to the complex regeneration processes and high energy cost (Avila et al., 2021a; Wang et al., 2021). Furthermore, the regeneration performance of PILs may be influenced by their high melting temperatures, density, and viscosity, posing additional challenges in their utilization (Fulvio and Dai, 2020; Wang et al., 2021).

### 3.2.8. Effect of aromatic hydrocarbon on extraction

The compositions of the real fuel are extremely complex. Particularly, a variety of aromatic hydrocarbons, polycyclic aromatic hydrocarbons are contained in diesel fuel (Luo et al., 2021; Xiong et al., 2020). The model fuels containing 20% paraxylene, phenanthrene and naphthalene (500 mg·kg<sup>-1</sup> of S for DBT) have been separately prepared to simulate the extractive desulfurization process of real fuel. The extraction results are shown in Fig. 5. The extraction efficiency of PPILs decreased slightly with the addition of paraxylene, phenanthrene and naphthalene. But it still maintained high extraction performance, indicating PPILs still achieves high extraction selectivity for DBT in the presence of polycyclic aromatic hydrocarbons. As a result, the PPILs may be an ideal extractant for desulfurization from fuel.

## 3.3. Extraction mechanism for PPILs

The extractive mechanism for PPILs is very essential for the industrialization. The FT-IR spectrum of PPILs before and after DBT extraction has been performed to investigate the interaction mechanism at 298 K. As shown in Fig. 6(a), the curves represent the IR results of DBT, PPILs and the mixture of PPILs respectively. The peak of 734 cm<sup>-1</sup> belongs to the bending vibration of C–H on the DBT (Jiang et al., 2015). Significantly, it's blue-shifted to 749 cm<sup>-1</sup> after interaction with PPILs. As far as we know, the DBT is an electron-withdrawing group (Liu et al., 2013; Ren et al., 2018). Therefore, it can be inferred that the increase in the absorption wave number of DBT is caused by the electron transfer from PPILs to

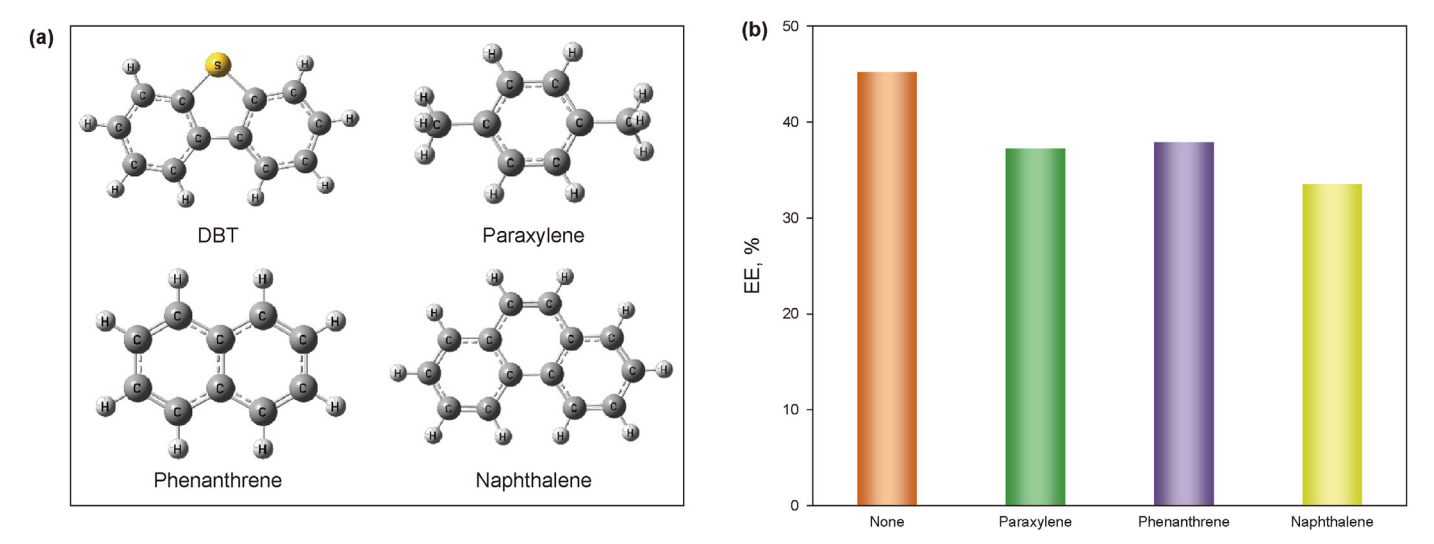


**Fig. 5.** (a) The structures of DBT, paraxylene, phenanthrene and naphthalene. (b) Extraction selectivity of DBT by PPILs, with added 20% paraxylene, phenanthrene and naphthalene to the model fuel, respectively. Experimental conditions: PPILs (m (PPILs); m (model fuel) = 1:5), T = 30 °C, t = 10 min.

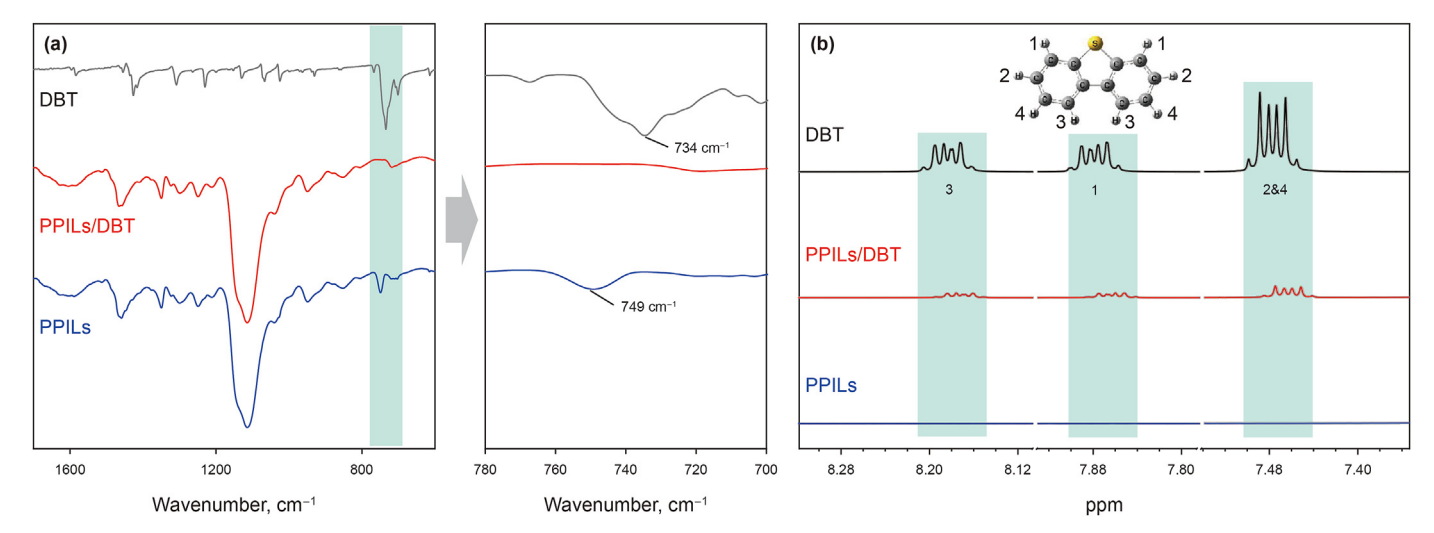


Fig. 6. (a) The FT-IR spectra of DBT, PPILs, and the mixture of PPILs and DBT. (b) Comparison of <sup>1</sup>H NMR spectrum between DBT, PPILs and the mixture of PPILs and DBT.

DBT. Besides, the <sup>1</sup>H NMR spectrum tests are also carried out to explore the extraction mechanism. As shown in Fig. 6(b), there are four types of aromatic hydrogen in the DBT structure, which are designated as 1, 2, 3 and 4, respectively. After the extraction process, the aromatic H peaks significantly shift to a higher field, which means the shielding effect and the electron density increase around them (Li et al., 2013; Moghadam et al., 2020). Therefore, it can be concluded that there is strong interaction (such as hydrogen bonding, van der Waals interaction and electrostatic interaction et al.) between PPILs and DBT.

To gain deep insight, DFT calculations have been performed based on the experimental results to obtain the role of the PPILs during the selective extraction process. To begin with, the model of HS-SC was subjected to theoretical simulations for the sake of simplicity in Fig. S2. Furthermore, three different conformations of PPILs are selected in Fig. S3 to seek the optimal structure. Compared with other conformations, PPILs-1 has the lowest energy and the most stable structure, which is selected for following extraction mechanism research. As shown in Fig. 7, two different interaction sites (Site 1 and Site 2) have been obtained between DBT and PPILs-1 based on

the possible interaction of the ion pair and  $\pi \cdots \pi$  sites. The result shows that both two sites showed strong interaction (E\_int\_(PPILs-1/Site1)) =  $-12.5~\text{kcal}\cdot\text{mol}^{-1}$ , E\_int\_(PPILs-1/Site2) =  $-16.2~\text{kcal}\cdot\text{mol}^{-1}$ ), indicating the ion pairs as an intermediate, display good mass transfer performance and excellent extraction ability for DBT.

The reduced density gradient (RDG) analysis has been proposed to analyze noncovalent interactions between compounds (Johnson et al., 2010; Zhu et al., 2016). The Multiwfn program was used to obtain the map of the non-covalent interaction site between the extractant and DBT generated using the Multiwfn program (Lu and Chen, 2012). In Fig. 7, the gradient isosurfaces (s=0.35 a.u.) for PPILs and DBT have been plotted. The process of changing from red to blue indicates the transition of non-covalent interaction between compounds from strong attractive interactions to nonbonded overlaps. The transition region represents typical hydrogen, van der Waals interaction and so on. It can be seen that there are various types of interaction between PPILs and DBT in Fig. 7. Among them, hydrogen bonding,  $\pi \cdots \pi$  and  $C-H \cdots \pi$  are dominant in the Brønsted acid-base site and the site in GAELE. In summary, RDG reveals that ion pairs have multiple extraction sites, indicating it

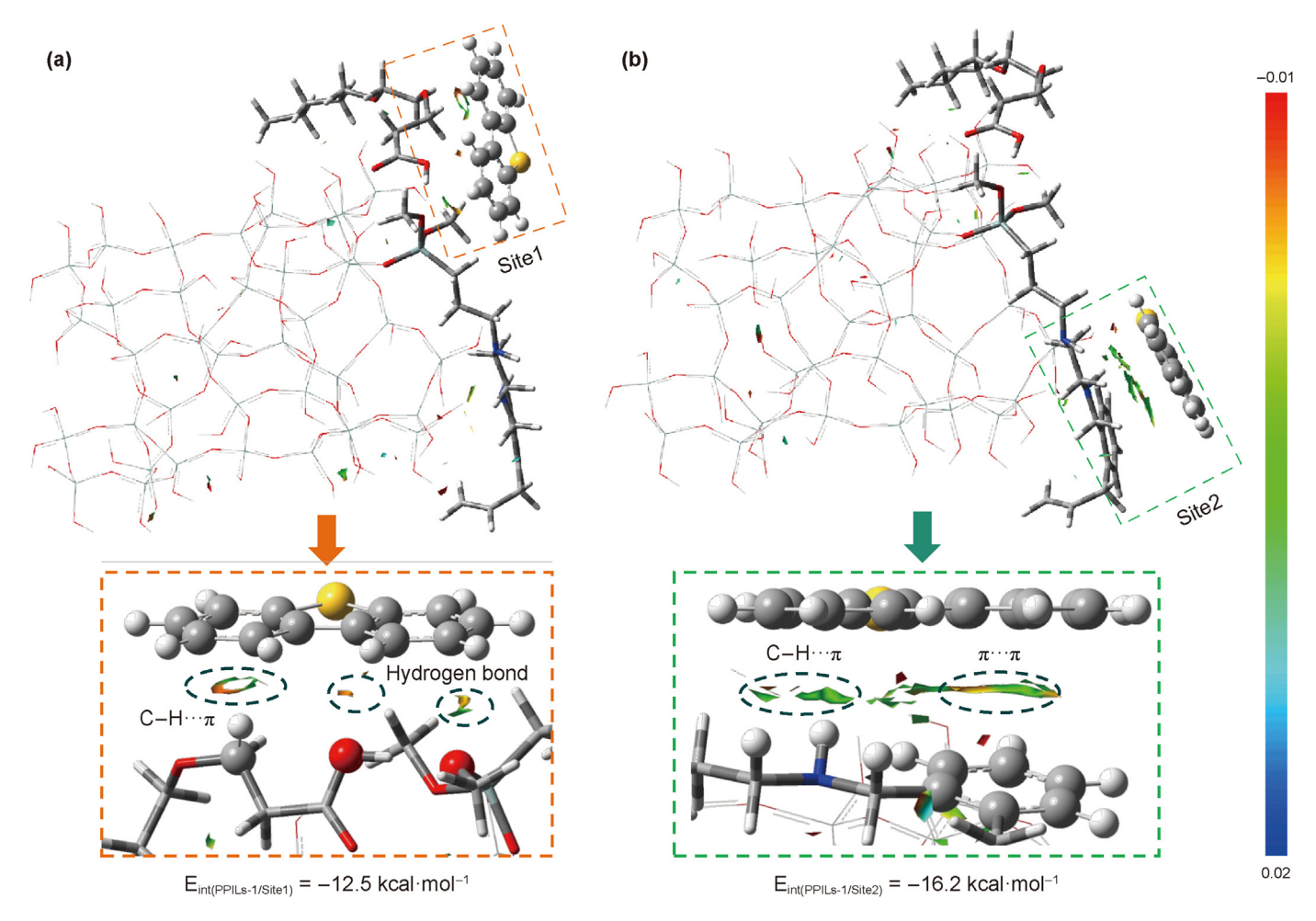


Fig. 7. Gradient isosurfaces (s = 0.35 a.u.) for PPILs and DBT. The surfaces are colored on a red-green-blue scale according to values of  $sign(\lambda_2)\rho$ , ranging from -0.01 to 0.02 a.u. The process of changing from red to blue indicates the transition of non-covalent interaction between compounds from strong attractive interactions to nonbonded overlaps.

plays an important role in the extraction desulfurization process, such as transport or capture of DBT.

To understand the selectivity of DBT as compared with other oil components, DFT calculations have been employed. Based on the experimental results, DBT, paraxylene, naphthalene and phenanthrene have been selected for the extraction selectivity test. The calculated results of HS-SC/DBT (-39.8 kcal·mol<sup>-1</sup>) showed stronger interaction energy than that in HS-SC/Paraxylene  $(-30.6 \text{ kcal} \cdot \text{mol}^{-1})$ , HS-SC/Naphthalene  $(-30.7 \text{ kcal} \cdot \text{mol}^{-1})$  and  $HS-SC/Phenanthrene (-29.6 kcal mol^{-1})$ , further reflecting the porous channels of PPILs has a fine selection for DBT in Fig. 8. The porous channels have stronger interaction energy for DBT compared with the ion pairs, indicating ion pairs are mainly transporters in the extractive process. Previous work has shown that the mechanism of EDS is dominated by the properties of the whole molecule (Li et al., 2016). Therefore, the electrophilicity index and Mulliken electronegativity of DBT, paraxylene, phenanthrene and naphthalene have been obtained by Mulliken (Li et al., 2016). These two conceptual DFT descriptors are estimations of the ability to gain electrons from different chemical considerations. As shown in Table 2, the DBT shows the highest electrophilicity index compared with phenanthrene, naphthalene, paraxylene. Besides, similar trends can be also found for Mulliken electronegativity. This result can be inferred that the PPILs takes on positive effects on the selectivity of DBT. In general, the HS has exceptional selectivity for DBT and the ion pairs has good mass transfer

performance besides the extraction ability in the PPILs extractive system. Based on the result above, the mechanism of the extractive process was proposed in Scheme 2. The DBT and some aromatic compounds was firstly enriched by the ion pair from the fuel phase, and then transported to porous structure while the HS selectively captures DBT into the porous channels. The DFT results indicate the presence of abundant interaction sites between ILs and DBT, with the main interaction modes being  $\pi\cdots\pi$ , C–H $\cdots\pi$  and hydrogen bonds etc. Additionally, the pore structure of HS exhibits a stronger interaction energy for the highly electrophilic DBT.

#### 4. Conclusion

A dual-functional protic porous ionic liquids (PPILs) with task-specific has been successfully prepared by OCNR method for the EDS process, exhibiting highly efficient extraction performance under mild conditions. A deep desulfurization efficiency of 95.6% was achieved after a multistage extraction process. Additionally, the PPILs exhibit excellent selectivity towards sulfur compounds. The results can be mainly attributed to the high specific surface area of the porous structure and the rapid mass transfer of ion pairs, as determined through experimental and theoretical analysis. Moreover, the porous channels with higher electrophilicity exhibit selectivity towards DBT, while the multiple extraction sites of ion pairs efficiently transport and capture DBT through various types of van der Waals interactions. In summary, the OCNR strategy

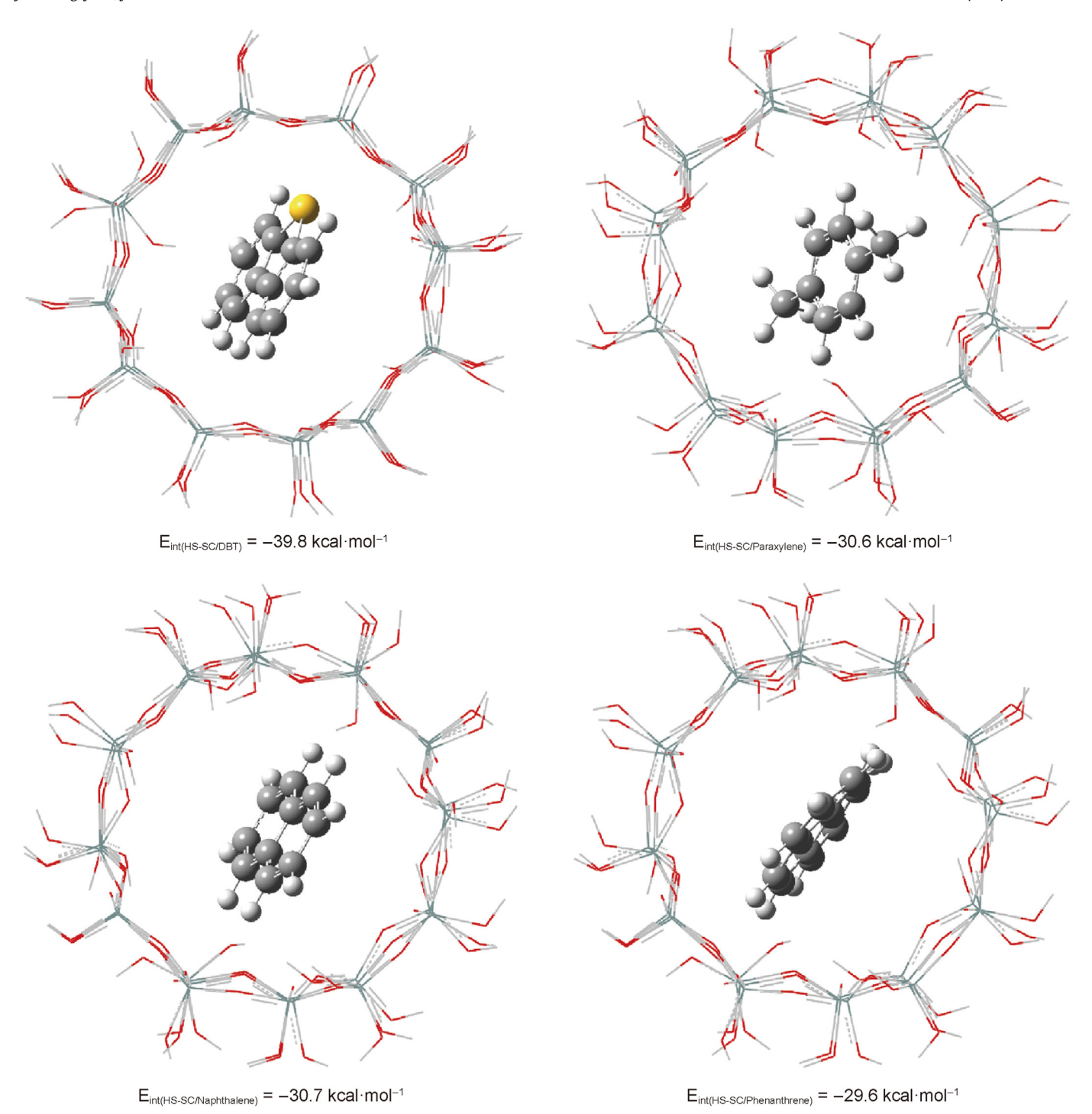


Fig. 8. The interaction energy between the channel of HS-SC and aromatic compounds (DBT, paraxylene, naphthalene and phenanthrene).

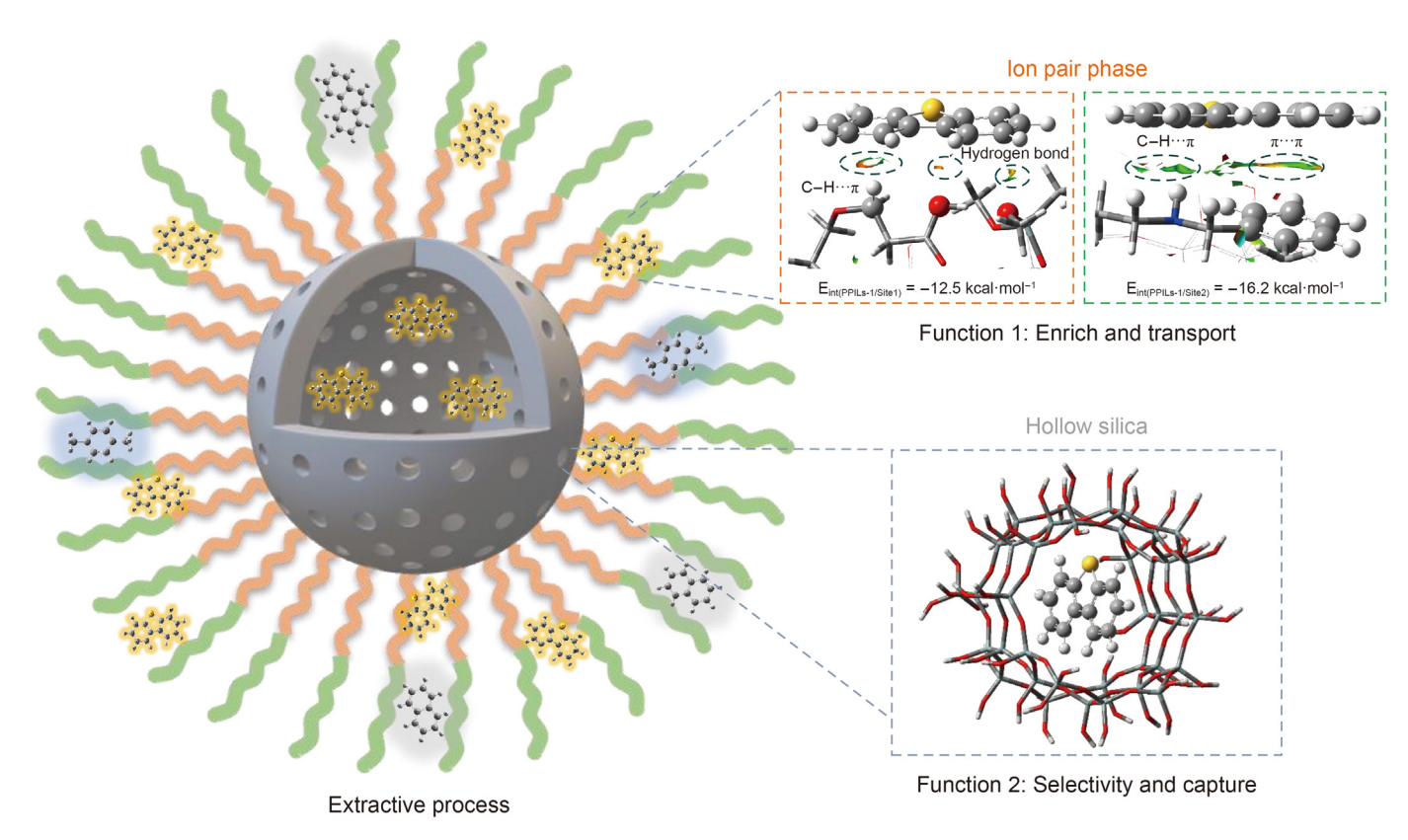
**Table 2**The electrophilicity index and Mulliken electronegativity of DBT, paraxylene, phenanthrene and naphthalene (Unit: a.u.).

	Electrophilicity index	Mulliken electronegativity
DBT	0.0258	0.1254
Naphthalene	0.0245	0.1246
Phenanthrene	0.0257	0.1238
Paraxylene	0.0156	0.1093

provides new possibilities for the synthesis of task-specific PILs extractants, inspiring further research in this field.

# **CRediT authorship contribution statement**

**Jin-Rui Zhang:** Writing — review & editing, Writing — original draft, Investigation, Formal analysis, Data curation. **Jie Yin:** Supervision, Investigation. **Jing He:** Supervision. **Hong-Shun Ran:** Formal analysis. **Wei Jiang:** Supervision. **Hong-Ping Li:** Writing — review &



Scheme 2. The mechanism of DBT extraction by PPILs.

editing, Software, Resources, Funding acquisition, Formal analysis. **Wen-Shuai Zhu:** Resources, Project administration. **Hua-Ming Li:** Project administration. **Ming Zhang:** Writing — review & editing, Project administration, Formal analysis.

# **Declaration of competing interest**

The authors declare that they have no known competing financial interests or personal relationships that could have appeared to influence the work reported in this paper.

## Acknowledgements

This work was financially supported by the National Natural Science Foundation of China (Nos. 22078135, 21808092, 21978119, 22202088).

# Appendix A. Supplementary data

Supplementary data to this article can be found online at https://doi.org/10.1016/j.petsci.2024.05.001.

## References

- Abro, R., Abdeltawab, A.A., Al-Deyab, S.S., et al., 2014. A review of extractive desulfurization of fuel oils using ionic liquids. RSC Adv. 4 (67), 35302—35317. https://doi.org/10.1039/c4ra03478c.
- Aghaei, A., Sobati, M.A., 2022. Extraction of sulfur compounds from middle distillate fuels using ionic liquids and deep eutectic solvents: a critical review. Fuel 310, 122279. https://doi.org/10.1016/j.fuel.2021.122279.
- Avila, J., Červinka, C., Dugas, P.Y., et al., 2021a. Porous ionic liquids: structure, stability, and gas absorption mechanisms. Adv. Mater. Interfac. 8 (9), 2001982. https://doi.org/10.1002/admi.202001982.
- Avila, J., Lepre, L.F., Santini, C.C., et al., 2021b. High-performance porous ionic liquids for low-pressure CO<sub>2</sub> Capture. Angew. Chem. Int. Ed. 60 (23), 12876–12882.

https://doi.org/10.1002/anie.202100090.

- Butt, H.S., Lethesh, K.C., Fiksdahl, A., 2020. Fuel oil desulfurization with dual functionalized imidazolium based ionic liquids. Sep. Purif. Technol. 248, 116959. https://doi.org/10.1016/j.seppur.2020.116959.
- Egleston, B.D., Mroz, A., Jelfs, K.E., et al., 2022. Porous liquids-the future is looking emptier. Chem. Sci. 13 (18), 5042–5054. https://doi.org/10.1039/d2sc00087c.
- El-Maghrabi, H.H., Mohamed, R.S., Younes, A.A., 2021. Reduction of sulfur oxides emissions via adsorptive desulfurization of transportation fuels using novel silica-based adsorbent. Environ. Sci. Pollut. Res. 28, 45933–45945. https://doi.org/10.1007/s11356-021-14039-6.
- Frisch, M.J., Trucks, G.W., Schlegel, H.B., et al., 2016. Gaussian 16 Rev. B.01.
- Fulvio, P.F., Dai, S., 2020. Porous liquids: the next frontier. Chem 6 (12), 3263—3287. https://doi.org/10.1016/j.chempr.2020.11.005.
- Gao, J., Zhu, S., Dai, Y., et al., 2018. Performance and mechanism for extractive desulfurization of fuel oil using modified polyethylene glycol. Fuel 233, 704–713. https://doi.org/10.1016/j.fuel.2018.06.101.
- Gautam, R., Kumar, N., Lynam, J.G., 2020. Theoretical and experimental study of choline chloride-carboxylic acid deep eutectic solvents and their hydrogen bonds. J. Mol. Struct. 1222, 128849. https://doi.org/10.1016/ j.molstruc.2020.128849.
- Greenaway, R.L., Holden, D., Eden, E.G.B., et al., 2017. Understanding gas capacity, guest selectivity, and diffusion in porous liquids. Chem. Sci. 8 (4), 2640–2651. https://doi.org/10.1039/c6sc05196k.
- Guo, Z., Jiang, Q., Shi, Y., et al., 2017. Tethering dual hydroxyls into mesoporous poly(ionic liquid)s for chemical fixation of CO<sub>2</sub> at ambient conditions: a combined experimental and theoretical study. ACS Catal. 7 (10), 6770–6780. https://doi.org/10.1021/acscatal.7b02399.
- Jiang, W., Xiao, J., Gao, X., et al., 2021. In situ fabrication of hollow silica confined defective molybdenum oxide for enhanced catalytic oxidative desulfurization of diesel fuels. Fuel 305, 121470. https://doi.org/10.1016/j.fuel.2021.121470.
- Jiang, W., Zhu, K., Li, H., et al., 2020. Synergistic effect of dual Brønsted acidic deep eutectic solvents for oxidative desulfurization of diesel fuel. Chem. Eng. J. 394, 124831. https://doi.org/10.1016/j.cej.2020.124831.
- Jiang, W., Zhu, W., Li, H., et al., 2015. Temperature-responsive ionic liquid extraction and separation of the aromatic sulfur compounds. Fuel 140, 590–596. https:// doi.org/10.1016/j.fuel.2014.09.083.
- Johnson, E.R., Keinan, S., Mori-Sanchez, P., et al., 2010. Revealing noncovalent interactions. J. Am. Chem. Soc. 132 (18), 6498–6506. https://doi.org/10.1021/ia100936w
- Kianpour, E., Azizian, S., 2014. Polyethylene glycol as a green solvent for effective extractive desulfurization of liquid fuel at ambient conditions. Fuel 137, 36–40. https://doi.org/10.1016/j.fuel.2014.07.096.

Kianpour, E., Azizian, S., Yarie, M., et al., 2016. A task-specific phosphonium ionic liquid as an efficient extractant for green desulfurization of liquid fuel: an experimental and computational study. Chem. Eng. J. 295, 500–508. https:// doi.org/10.1016/j.cej.2016.03.072.

- Koyama, Y., Ikeda, T., Tatsumi, T., et al., 2008. A multi-dimensional microporous silicate that is isomorphous to Zeolite MCM-68. Angew. Chem. Int. Ed. 120 (6), 1058–1062. https://doi.org/10.1002/ange.200704222.
- Li, C., Li, D., Zou, S., et al., 2013. Extraction desulfurization process of fuels with ammonium-based deep eutectic solvents. Green Chem. 15 (10), 2793. https:// doi.org/10.1039/c3gc41067f.
- Li, H., Zhang, B., Jiang, W., et al., 2019. A comparative study of the extractive desulfurization mechanism by Cu(II) and Zn-based imidazolium ionic liquids. Green Energy Environ. 4 (1), 38–48. https://doi.org/10.1016/j.gee.2017.10.003.
- Li, H., Zhu, W., Zhu, S., et al., 2016. The selectivity for sulfur removal from oils: an insight from conceptual density functional theory. AIChE J. 62 (6), 2087—2100. https://doi.org/10.1002/aic.15161.
- Li, P., Wang, D., Zhang, L., et al., 2021. An in situ coupling strategy toward porous carbon liquid with permanent porosity. Small 17 (10), e2006687. https:// doi.org/10.1002/smll.202006687.
- Li, Z., Li, C., Chi, Y., et al., 2012. Extraction process of dibenzothiophene with new distillable Amine-based protic ionic liquids. Energy Fuels 26 (6), 3723–3727. https://doi.org/10.1021/ef3005064.
- Li, Z., Xu, J., Li, D., et al., 2015. Extraction process of sulfur compounds from fuels with protic ionic liquids. RSC Adv. 5 (21), 15892—15897. https://doi.org/10.1039/c4ra16186f
- Liu, D., Ren, H., Deng, L., et al., 2013. Synthesis and electrophosphorescence of iridium complexes containing benzothiazole-based ligands. ACS Appl. Mater. Interfaces 5 (11), 4937–4944. https://doi.org/10.1021/am400672y.
- Lu, T., Chen, F., 2012. Multiwfn: a multifunctional wavefunction analyzer. J. Comput. Chem. 33 (5), 580–592. https://doi.org/10.1002/jcc.22885.
- Luo, J., Chao, Y., Tang, Z., et al., 2019. Design of lewis acid centers in bundlelike boron nitride for boosting adsorptive desulfurization performance. Ind. Eng. Chem. Res. 58 (29), 13303–13312. https://doi.org/10.1021/acs.iecr.9b01745.
- Res. 58 (29), 13303–13312. https://doi.org/10.1021/acs.iecr.9b01745.
  Luo, J., Wang, C., Liu, J.X., et al., 2021. High-performance adsorptive desulfurization by ternary hybrid boron carbon nitride aerogel. AIChE J. 67 (9), e17280. https://doi.org/10.1002/aic.17280.
- Lv, N., Sun, L., Chen, L., et al., 2019. The mechanism of thiophene oxidation on metal-free two-dimensional hexagonal boron nitride. Phys. Chem. Chem. Phys. 21 (39), 21867–21874. https://doi.org/10.1039/c9cp03758f.
- Lv, N., Zhang, J., Yin, J., et al., 2022. Atomic Cu and Ni anchoring on h-BN for O<sub>2</sub> activation and subsequent oxidative desulfurization. Catal. Commun. 170, 106492. https://doi.org/10.1016/j.catcom.2022.106492.
- Ma, L., Haynes, C.J.E., Grommet, A.B., et al., 2020. Coordination cages as permanently porous ionic liquids. Nat. Chem. 12 (3), 270–275. https://doi.org/10.1038/s41557-020-0419-2.
- Meng, X., Zhou, P., Li, L., et al., 2020. A study of the desulfurization selectivity of a reductive and extractive desulfurization process with sodium borohydride in polyethylene glycol. Sci. Rep. 10 (1), 10450. https://doi.org/10.1038/s41598-020-67235.
- Moghadam, F.R., Kianpour, E., Azizian, S., et al., 2020. Extractive desulfurization of liquid fuel using diamine-terminated polyethylene glycol as a very low vapour pressure and green molecular solvent. R. Soc. Open Sci. 7 (11), 200803. https://doi.org/10.1098/rsos.200803.
- Rajendran, A., Cui, T., Fan, H., et al., 2020. A comprehensive review on oxidative desulfurization catalysts targeting clean energy and environment. J. Mater. Chem. A 8 (5), 2246–2285. https://doi.org/10.1039/c9ta12555h.
- Ramenskaya, L.M., Grishina, E.P., Kudryakova, N.O., 2020. Comparative study of atmospheric ionic liquids based on bis(trifluoromethylsulfonyl)imide anion and alkyl substituted cations of ammonium, pyrrolidinium and imidazolium. J. Mol. Liq. 312, 113368. https://doi.org/10.1016/j.molliq.2020.113368.
- Ren, Z., Zhou, Z., Li, M., et al., 2018. Deep desulfurization of fuels using imidazole Anion-based ionic liquids. ACS Sustain. Chem. Eng. 7 (2), 1890–1900. https://doi.org/10.1021/acssuschemeng.8b03566.
- Ribeiro, D.C.M., Rebelo, R.C., De Bon, F., et al., 2021. Process development for flexible films of industrial cellulose pulp using superbase ionic liquids. Polymers 13 (11), 1767. https://doi.org/10.3390/polym13111767.
- Salah, H.B., Nancarrow, P., Al-Othman, A., 2021. Ionic liquid-assisted refinery processes a review and industrial perspective. Fuel 302, 121195. https://doi.org/10.1016/ji.fuel.2021.121195.
- Smith, E.L., Abbott, A.P., Ryder, K.S., 2014. Deep eutectic solvents (DESs) and their applications. Chem. Rev. 114 (21), 11060–11082. https://doi.org/10.1021/cr300162p.
- Sudhir, N., Yadav, P., Nautiyal, B.R., et al., 2019. Extractive desulfurization of fuel with methyltriphenyl phosphonium bromide- tetraethylene glycol-based eutectic solvents. Separ. Sci. Technol. 55 (3), 554–563. https://doi.org/10.1080/ 01496395.2019.1569061.
- Wang, D., Xin, Y., Yao, D., et al., 2021. Shining light on porous liquids: from fundamentals to syntheses, applications and future challenges. Adv. Funct. Mater. 32 (1), 2104162. https://doi.org/10.1002/adfm.202104162.
- Wang, H., Liu, S., Zhao, Y., et al., 2019. Insights into the hydrogen bond interactions

- in deep eutectic solvents composed of choline chloride and polyols. ACS Sustain. Chem. Eng. 7 (8), 7760–7767. https://doi.org/10.1021/acssuschemeng.8b06676.
- Wang, H., Tang, M., Shi, F., et al., 2020. Amorphous Cr<sub>2</sub>WO<sub>6</sub>-Modified WO<sub>3</sub> nanowires with a large specific surface area and rich Lewis acid sites: a highly efficient catalyst for oxidative desulfurization. ACS Appl. Mater. Interfaces 12 (34), 38140–38152. https://doi.org/10.1021/acsami.0c10118.
- Wang, Q., Zhang, T., Zhang, S., et al., 2020. Extractive desulfurization of fuels using trialkylamine-based protic ionic liquids. Sep. Purif. Technol. 231, 115923. https://doi.org/10.1016/j.seppur.2019.115923.
- Wang, X., Jiang, W., Zhu, W., et al., 2016. A simple and cost-effective extractive desulfurization process with novel deep eutectic solvents. RSC Adv. 6 (36), 30345–30352. https://doi.org/10.1039/c5ra27266a.
- Wu, J., Wu, X., Zhao, P., et al., 2021. Extraction desulphurization of fuels using ZIF-8-based porous liquid. Fuel 300, 121013. https://doi.org/10.1016/i.fuel.2021.121013.
- Xiong, J., Luo, J., Di, J., et al., 2020. Macroscopic 3D boron nitride monolith for efficient adsorptive desulfurization. Fuel 261, 116448. https://doi.org/10.1016/ ifinel 2019 116448
- Xu, L.X., Luo, Y.P., Liu, H., et al., 2021. Extractive desulfurization of diesel fuel by amide-based type IV deep eutectic solvents. J. Mol. Liq. 338. https://doi.org/ 10.1016/j.molliq.2021.116620.
- Yin, J., Fu, W., Zhang, J., et al., 2023. UiO-66(Zr)-based porous ionic liquids for highly efficient extraction coupled catalytic oxidative desulfurization. Chem. Eng. J. 470, 144290. https://doi.org/10.1016/j.cej.2023.144290.
- Yin, J., Zhang, J., Fu, W., et al., 2021. Theoretical prediction of the SO(2) absorption by hollow silica based porous ionic liquids. J. Mol. Graph. Model. 103, 107788. https://doi.org/10.1016/j.jmgm.2020.107788.
- Yin, J., Zhang, J., Fu, W., et al., 2022. Porous liquids for gas capture, separation, and conversion: narrowing the knowing-doing gap. Sep. Purif. Technol. 297, 121456. https://doi.org/10.1016/j.seppur.2022.121456.
- Yu, F., Liu, C., Yuan, B., et al., 2016. Energy-efficient extractive desulfurization of gasoline by polyether-based ionic liquids. Fuel 177, 39–45. https://doi.org/ 10.1016/j.fuel.2016.02.063.
- Yuzbashi, S., Mousazadeh, M.H., Ramezani, N., et al., 2020. Mesoporous zirconiumsilica nanocomposite modified with heteropoly tungstophosphoric acid catalyst for ultra-deep oxidative desulfurization. Appl. Organomet. Chem. 34 (2), e5326. https://doi.org/10.1002/aoc.5326.
- Zeng, X., Mo, G., Wang, H., et al., 2014. Oxidation mechanism of dibenzothiophene compounds: a computational study. Comput Theor Chem 1037, 22–27. https:// doi.org/10.1016/j.comptc.2014.03.023.
- Zhang, J., Chai, S.H., Qiao, Z.A., et al., 2015. Porous liquids: a promising class of media for gas separation. Angew. Chem. Int. Ed. 54 (3), 932–936. https://doi.org/10.1002/anie.201409420.
- Zhang, J., Lv, N., Chao, Y., et al., 2020. The interaction nature between hollow silicabased porous ionic liquids and CO<sub>2</sub>: a DFT study. J. Mol. Graph. Model. 100, 107694. https://doi.org/10.1016/j.jmgm.2020.107694.
- Zhang, J., Yin, J., Fu, W., et al., 2023a. Highly efficient extractive desulfurization by specific functionalized porous ionic liquids via  $C-H\cdots\pi$  interactions. Fuel Process. Technol. 243, 107687. https://doi.org/10.1016/j.fuproc.2023.107687.
- Zhang, J., Yin, J., Zhang, X., et al., 2023b. Constructing protic porous ionic liquids via one-step coupling neutralization reaction for extraction-adsorption coupled desulfurization. J. Colloid Interface Sci. 652, 1836—1847. https://doi.org/10.1016/j.jcis.2023.09.004.
- Zhang, J., Yin, J., Zhang, Y., et al., 2022. Insights into the formation mechanism of aliphatic acid-choline chloride deep eutectic solvents by theoretical and experimental research. J. Mol. Liq. 367, 120342. https://doi.org/10.1016/ j.molliq.2022.120342.
- Zhang, M., Liao, W.Y., Wei, Y.C., et al., 2021. Aerobic oxidative desulfurization by nanoporous tungsten oxide with oxygen defects. ACS Appl. Nano Mater. 4 (2), 1085–1093. https://doi.org/10.1021/acsanm.0c02639.
- Zhang, P., Mao, X., Mi, R., et al., 2020. Mesoporous silica encapsulated phosphotungstic acid catalysts for alkylation desulfurization of gasoline. Catal. Lett. 15 (1), 95–106. https://doi.org/10.1007/s10562-020-03288-8.
- Zhang, T., Doert, T., Wang, H., et al., 2021. Inorganic synthesis based on reactions of ionic liquids and deep eutectic solvents. Angew. Chem. Int. Ed. 60, 2–20. https://doi.org/10.1002/anie.202104035.
- Zhao, H., Baker, G.A., Wagle, D.V., et al., 2016. Tuning Task-specific ionic liquids for the extractive desulfurization of liquid fuel. ACS Sustain. Chem. Eng. 4 (9), 4771–4780. https://doi.org/10.1021/acssuschemeng.6b00972.
- Zhou, Y., Avila, J., Berthet, N., et al., 2021. Integrated, one-pot carbon capture and utilisation using porous ionic liquids. Chem. Commun. 57 (64), 7922–7925. https://doi.org/10.1039/d1cc02642a.
- Zhu, S., Cheng, H., Dai, Y., et al., 2020. Extractive desulfurization and denitrogenation from fuel oil by a Polyether-amine-based solvent. Energy Fuels 34 (7), 8186–8194. https://doi.org/10.1021/acs.energyfuels.0c01096.
- Zhu, S., Li, H., Zhu, W., et al., 2016. Vibrational analysis and formation mechanism of typical deep eutectic solvents: an experimental and theoretical study. J. Mol. Graph. 68, 158–175. https://doi.org/10.1016/j.jmgm.2016.05.003.